# Topological skin modes and intensity amplification in a nonlinear non-Hermitian lattice

Zhi-Xu Zhang,[1] Ji Cao,[2] Jing-Quan Li,[2] Yu Zhang,[1,*] Shutian Liu,[1,†] Shou Zhang,[2] and Hong-Fu Wang[2,‡]
[1]*School of Physics, Harbin Institute of Technology, Harbin, Heilongjiang 150001, China*
[2]*Department of Physics, College of Science, Yanbian University, Yanji, Jilin 133002, China*

(Received 10 May 2023; revised 14 August 2023; accepted 22 August 2023; published 5 September 2023)

Topological lattice systems combined with nonlinearity and non-Hermiticity can give rise to novel solitons, whose exceptional properties are demonstrated in both unique quench dynamics and topological boundary states. Especially, we focus on an Aubry-André-Harper-type lattice with nonlinear hopping and demonstrate its ability to host distinct topological soliton states in the short-run regime and intensity amplification in the long-run regime. Actually, these topological soliton states arise from the competition between nonreciprocal hopping and on-site modulation, resulting in an alternating dominance between the skin effect and Anderson localization. Notably, we find that the site intensities near the edge of the lattice are strongly enhanced in the long-run regime due to the combination of nonlinearity and the non-Hermitian skin effect, which distinguishes it from the previously studied nonlinear lattices. To reveal the intensity amplification effect in more detail, we explore a time-dependent intensification factor and find that the amplification effect is more pronounced in the long-run regime. Our results demonstrate the promising possibilities of combining nonlinearity and non-Hermiticity in topological lattice systems to develop novel solitons with exceptional properties.

DOI: 10.1103/PhysRevB.108.125402

## I. INTRODUCTION

A consistent theme in condensed matter physics has been the discovery and classification of distinct topological phases of matter, in which the avenues for tackling the issues of topological physics have reshaped our perspective of non-Hermitian systems [1–6]. Recently, there has been growing interest in non-Hermitian topological systems, which exhibit sensitivity to boundary conditions due to their complex energy spectra. This sensitivity is in sharp contrast to the Hermitian case and is caused by nonreciprocal hopping or complex on-site gain/loss [7–11]. The non-Hermiticity profoundly affects traditional topological properties and has been extensively investigated, leading to the discovery of non-Hermitian skin effects (NHSEs), exceptional points, and the breakdown of traditional bulk-boundary correspondence [12–19]. Remarkably, extensive efforts originating from both complex band structures and skin boundary modes have reached the same conclusion: non-Hermiticity profoundly extends the realm of topological physics into open systems that interact with the environment, but not closed systems [20–25].

However, current non-Hermitian theoretical issues are restricted to linear topological regimes and guaranteed system symmetries, thereby underestimating the complexity of non-Hermitian topological systems induced by nonreciprocal hopping and complex on-site potentials, mixed boundary conditions, and Floquet topological dynamics [26–28]. This situation has significantly improved through recent efforts that combine nonreciprocal hopping and nonlinear systems. Considerable attempts have been made to investigate these enigmatic nonlinear non-Hermitian boundary modes, which are found to be conclusive in various physical systems [29–35]. Nonlinearity also plays a role in nonlinear on-site modulation and higher-order topological systems, revealing macroscopic, but counterintuitive, topological properties that are more difficult to understand [36–40]. Meanwhile, extensive experiments have shown that nonlinear interactions have been successfully implemented and studied in various platforms such as nonlinear optics [41–44], nonlinear circuits [31,38,45,46], and nonlinear mechanical lattices [47–50]. Among these endeavors, we should point out that Lang *et al.* [38] analyzed in detail the non-Hermitian Su-Schrieffer-Heeger (SSH)-type lattice with nonlinear hopping and discovered a novel and intriguing phenomenon called the "topological end breather." Nevertheless, a key question is whether such a phenomenon appears only in one class of SSH models due to the existence of special end states under open boundary conditions and whether the end breather can maintain a stable form over a prolonged evolution.

Motivated by the ideas mentioned above, in this paper, we explore the behavior of a one-dimensional nonlinear non-Hermitian Aubry-André-Harper (AAH) lattice subjected to edge-site stimulation. We demonstrate that the lattice can support oscillatory edge-localized modes in the short-run regime and intensity amplification in the long-run regime. Although these modes are similar to the topological end breather discovered in the nonlinear non-Hermitian SSH model [38], their forming essence is vastly different. The topological end breather originates from the competition between topologically trivial and nontrivial phases, while the oscillatory and localized skin modes in our paper emerge from the

*zhangyunn@hit.edu.cn
†stliu@hit.edu.cn
‡hfwang@ybu.edu.cn

 

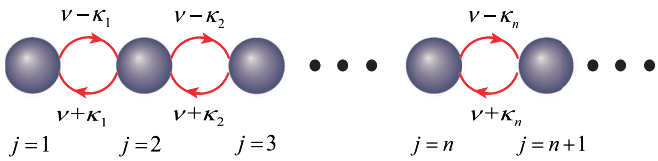


FIG. 1. Schematic diagram of the AAH lattice with both nonlinearity and nonreciprocal non-Hermiticity under the open boundary condition. The nonlinear nonreciprocal hopping between sites $j = n$ and $j = n + 1$ are represented as $\nu \pm \kappa_n$, and the on-site potential for site $j = n$ is denoted by $\Delta_n$.

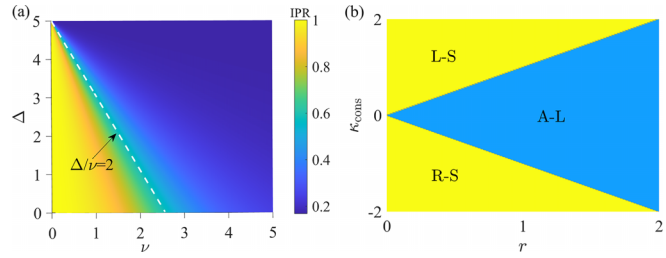


FIG. 2. (a) The IPR of the eigenstates as a function of hopping strengths $\nu$ and the on-site modulation amplitude $\Delta$ for the Hamiltonian in Eq. (1) with $\kappa_n = 0$, $\alpha = 5/8$, $N = 8$, and $\theta = 0$. (b) Phase diagram of skin and Anderson localized phases. The phase boundaries are determined by $r = \pm\kappa_{\text{cons}}$ ($r = \Delta/2 - \nu$). L-S (R-S) and A-L denote the left-skin (right-skin) and Anderson localized phases under the open boundary condition, respectively.

alternating dominance between Anderson localization and skin effects. Meanwhile, the competition between the on-site potential and nonreciprocal hopping leads to the appearance of these engrossing edge-localized modes. In addition, we reveal that by adjusting the modulation phase of the on-site potential, the topological skin modes can undergo a process of vanishing, emergence, and recovery. Notably, we reveal a neglected result in the long-run regime, in which the stable oscillatory topological skin mode vanishes and the edge-site intensities in the moment of final evolution are much greater than that in the initial moment. This phenomenon has not been mentioned in other studies, including those on pointlike topological solitons [44,47,48], topological end breathers [38], and higher-order nonlinear topological lasers [32,42]. Moreover, we define the intensity amplification factor to reveal the parametric relationship between the initial and final intensities; the result demonstrates that the amplification effect appears only in the long-run regime and not in the short-run case. This phenomenon indicates the generality of amplification effects in nonlinear systems and the potential for topological lattices with nonlinearity and non-Hermiticity to be devices for topological amplifiers and repeaters.

This paper is organized as follows: In Sec. II, we present the model and Hamiltonian. In Sec. III, the oscillatory and localized skin modes induced by nonlinear hopping are depicted and analyzed. In Sec. IV, the incomplete end breather theory and topological amplifier effect in the long-run regime are investigated and discussed. Finally, we provide a conclusion in Sec. V.

## II. SYSTEM AND HAMILTONIAN

Inspired by studies about nonlinear topological systems [13,31,38], we consider a one-dimensional non-Hermitian AAH lattice with nearest-neighbor nonlinear hopping, as depicted in Fig. 1. In the presence of the on-site modulation potential, the total tight-binding Hamiltonian is written as

$$H = \sum_{n=1}^{N-1}[(\nu - \kappa_n)c_{n+1}^{\dagger}c_n + (\nu + \kappa_n)c_n^{\dagger}c_{n+1}] + \sum_{n=1}^{N}\Delta_n c_n^{\dagger}c_n, \tag{1}$$

where $c_n^{(\dagger)}$ is the annihilation (creation) operator for $n$th site. The first two terms of the Hamiltonian denote the hopping between adjacent lattice sites with nonreciprocal strength $\nu \pm \kappa_n$, in which $\nu$ and $\kappa_n$ are real and site-dependent nonlinear hopping coefficients, respectively. The last term represents the on-site modulation potential $\Delta_n = \Delta\cos(2\pi\alpha n + \theta)$, where $\Delta$ and $\theta$ are the on-site modulation amplitude and phase factor and $\alpha$ is a positive and rational (irrational) number. For the limited system under open boundary conditions with lattice size $N = F_{n+1}$, if $F_n$ is the $n$th number in the Fibonacci sequence, $\alpha$ is usually determined as $\alpha = F_n/F_{n+1}$ (an irrational number) for the quasiperiodic case. And $\alpha$ is a rational number in the periodic case.

In the Hermitian limitation ($\kappa_n = 0$), the lattice degenerates to a standard AAH model with the Anderson localization occurring at $\Delta/\nu = 2$ because of the self-duality. This critical phase transition condition divides the localization states into two parts [51,52]: the extended and localized states for $\Delta/\nu < 2$ and $\Delta/\nu > 2$, respectively. This critical condition can be confirmed by computing the inverse participation ratio, $\text{IPR} = \sum_n |\psi_n|^4/(\sum_n |\psi_n|^2)^2$, where larger values of the IPR indicate localized states and smaller ones correspond to the extended states. In Fig. 2(a), we demonstrate that an obvious dividing line $\Delta/\nu = 2$ appears and separates the localized and extended states. Moreover, the exponentially localized state has the form $|\psi\rangle \propto \sum_n e^{-\xi|n-n_0|}|n\rangle$, which indicates its amplitude is involved with the localization center $n_0$ and Lyapunov exponent $\xi = \ln(\Delta/\nu)$ [13].

If the nonlinear terms $\kappa_n \neq 0$ but a constant $\kappa_n = \kappa_{\text{cons}}$, the model reduces to a generalized AAH model with nonreciprocal hopping. Significantly, under open boundary conditions, we find phase transitions of NHSEs and Anderson localization with an analytically reshaped solution $\Delta/\max(\nu \pm \kappa_{\text{cons}}) = 2$, which originates from the Hermitian counterpart, as mentioned before [13,16,45]. Moreover, we show this critical phase transition condition in Fig. 2(b) under open boundary conditions, where the blue region denotes the Anderson localized phase and the yellow regions L-S ($\kappa_{\text{cons}} > 0$) and R-S ($\kappa_{\text{cons}} < 0$) correspond to the left-skin and right-skin phases, respectively [13]. Because of the nonreciprocal hopping, the asymmetric Anderson localized states tend to be center dependent, apart from the NHSEs under open boundary conditions.

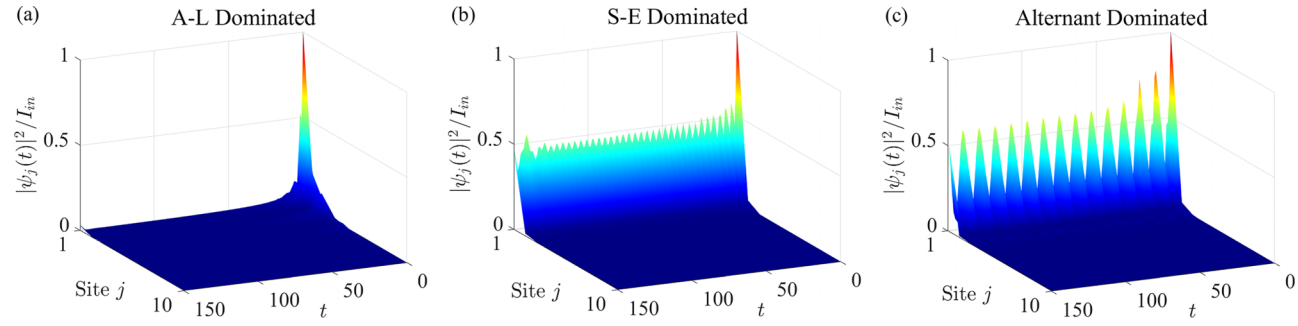


FIG. 3. [(a)–(c)] The site intensities evolve with time sustained in an edge-site stimulation, and the size of system is selected as $j = 100$. (a) The edge-site stimulation decays rapidly to zero, and the parameters are determined as $\kappa_0 = 0$, $\kappa_s = 0.3$, $\Delta = 2.8$, and $\alpha = \sqrt{2.2501}$. (b) The steady-state skin mode is generated, in which $\kappa_0 = 0.3$, $\kappa_s = 0.7$, $\Delta = 0.7$, and $\alpha = 6/5(\sqrt{5} - \sqrt{3})$. (c) The end breather-like induced by alternating dominance between A-L and S-E appears with $\kappa_0 = 0.3$, $\kappa_s = 0.7$, $\Delta = 3.2$, and $\alpha = 3/10(\sqrt{5} - \sqrt{3})$. Other parameters are set as $I_{\text{in}} = 10^3 I_s$, $\nu = 1$, $\theta = 1.41\pi$, and $I_s = 1$ for [(a)–(c)].

## III. SKIN MODES INDUCED BY NONLINEAR NONRECIPROCAL HOPPING IN THE SHORT-RUN REGIME

### A. Skin modes induced by nonlinear nonreciprocal hopping

To focus on the nonlinear case, the factitious alterable nonlinear hopping is selected as [38]

$$\kappa_n = \kappa_s - \frac{\kappa_s - \kappa_0}{1 + I_n(t)/I_s}, \tag{2}$$

where $\kappa_s$ and $I_s$ are adaptable real constants and saturation intensity scales, respectively. The intensity of termination evolution is interpreted as $I_n(t) \equiv |\psi_n(t)|^2$, where $\psi_n(t)$ denotes the time-dependent wave function for the $n$th site. Subsequently, we can observe that $\kappa_n \to \kappa_0$ under the zero-intensity limitation [i.e., $I_n(t) \to 0$] and $\kappa_n \to \kappa_s$ under the high-intensity limitation [i.e., $I_n(t) \to \infty$], which indicates the nonlinear hopping satisfies $\kappa_n \in [\kappa_0, \kappa_s)$ when $\kappa_s > \kappa_0$. In the linear regime, the appearance of NHSEs and Anderson localization in the non-Hermitian AAH model is relevant to the phase transition point $\Delta = 2\max(\nu + \kappa_n, \nu - \kappa_n)$. Thus, in the nonlinear regime, Anderson localization and its behavior are extensively subordinate to the nonlinear critical values $\kappa_c = -(\nu - \Delta/2)$ for $\kappa_n > 0$ and $\kappa_c = \nu - \Delta/2$ for $\kappa_n < 0$. It is worth noting that the definition of $\kappa_n$ in Eq. (2) imposes the constraint that $\kappa_n \geqslant 0$ (although $\kappa_n = 0$ has been considered before for the Hermitian case), which implies the critical value $\kappa_c = -(\nu - \Delta/2)$. Before delving into a comprehensive analysis, one non-negligible perspective is that $\sum_n I_n(t)$ is not conserved in the non-Hermitian case, and the terminal intensity may surpass the initial stimulation after a period of evolution [8,18,38].

We now turn to investigate the nonlinear nonreciprocal AAH model with the first site stimulation, whose initial state can be defined as $|\psi(0)\rangle = |\sqrt{I_{\text{in}}}, 0, 0, \ldots, 0, 0\rangle$ and whose evolution is governed by the nonlinear Hamiltonian in Eq. (1). The dynamical behavior of Anderson localization and NHSEs is investigated under three distinct parameter regimes of interest. Conceptually, high and low site occupied intensities correspond to the localized and extended cases, respectively. In case I, for $\kappa_0 < \kappa_s < \kappa_c$, each nonlinear hopping $\kappa_n$ is below the critical value $\kappa_c$, and a swift attenuation of the initial stimulation appears, as shown in Fig. 3(a). The reason is that edge-site stimulation diffuses into the bulk due to the dominance of the Anderson localization, leading to the decreasing of edge-site intensity over the evolution until it vanishes. In case II, for $\kappa_c < \kappa_0 < \kappa_s$, all nonlinear hoppings $\kappa_n$ are above the threshold, and the initial stimulation generates a steady-state skin mode localized at the boundary, as shown in Fig. 3(b). The reason is that the instantaneous system is dominated by the skin effect, and the eigenstates are inherently localized on the boundary even without stimulation.

Among these regimes, case III, in which nonlinear hopping $\kappa_0 < \kappa_c < \kappa_s$, demonstrates fascinating discoveries. As shown in Fig. 3(c), the edge-site simulation motivates a self-sustained oscillation around the boundary, which we refer to as "end breather-like." It is noteworthy that this type of skin mode is only similar in appearance to the end breather proposed by Ref. [38] and is fundamentally distinctive. The appearance of an end breather is induced by the competition between topologically trivial and nontrivial phases, depending on instantaneous inter- or intracell hopping. However, in the nonreciprocal AAH model, the competition between on-site modulation and nonreciprocal hopping allows for the alternating appearance of the skin and Anderson localized phases, leading to the subsistence of end breather-like. We notice that the non-Hermitian skin effect plays a crucial role in the emergence of these end modes, despite the distinct intrinsic factors between the end breather-like and end breather.

It is noteworthy that Lang's proposition in Ref. [38] regarding the behavior of the end breather is intricately linked to independent nonreciprocal hoppings. The skin effect can be explained as the inhibitory effect of similarity transformations of the eigenfunctions of non-Hermitian systems, effectively constraining their deviation from the system boundary. In our research, we are actively investigating the potential expansion of the approach based on the similarity transformations matrix $S$ while considering the independence of intensity parameters $\kappa_1$, $\kappa_2$, $\kappa_3$, .... By employing distinct similarity transformation matrices $S$, we can establish a profound relationship between the non-Hermitian Hamiltonian $H$ and a corresponding Hermitian Hamiltonian $H_h$, represented as $H = SH_hS^{-1}$, where the position basis in our study can be accurately

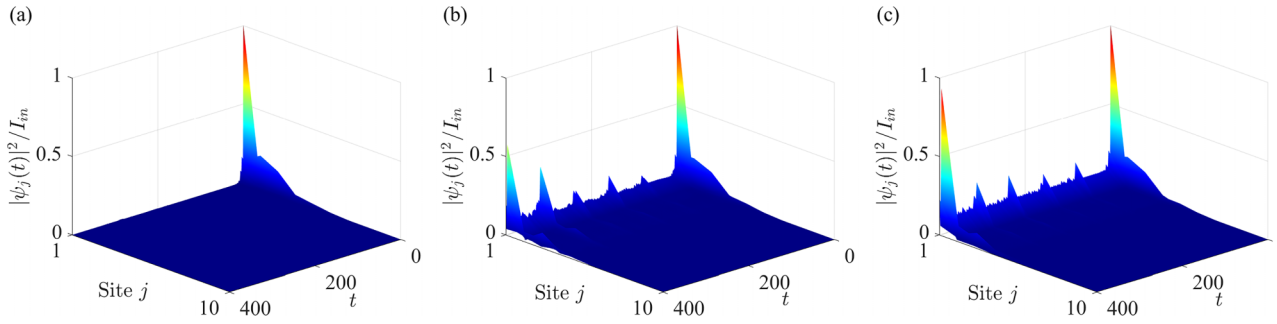


FIG. 4. The site intensities evolve with time. [(a)–(c)] Skin modes corresponding to $\theta = 0$, $\theta = 0.3\pi$, and $\theta = 0.5\pi$, respectively. Other parameters are set as $\nu = 1$, $\kappa_0 = 0$, $\Delta = 0.5$, $\alpha = 0.4$, and $\kappa_s = 0.5$.

denoted as

$$S = \mathrm{diag}[1, \lambda_1, \lambda_1\lambda_2, \lambda_1\lambda_2\lambda_3, \lambda_1\lambda_2\lambda_3\lambda_4, \dots],$$
$$\lambda_n = \sqrt{\frac{\nu - \kappa_n}{\nu + \kappa_n}} < 1. \tag{3}$$

### B. The revival of skin modes induced by on-site modulation

It is widely known that the Anderson localization of the AAH model in the noninteraction regime is determined by the nearest-neighbor hopping and on-site modulation, regardless of whether the system is Hermitian or non-Hermitian. Motivated by this perspective, we investigated how on-site modulation affects the skin modes with edge-site stimulation. The result of the initial edge-site stimulation with $\theta = 0$ is shown in Fig. 4(a), where the localized effect occurs only at the beginning of evolution, consistent with the phenomenon in Fig. 3(a). With the alteration of the on-site modulation phase $\theta = 0.3\pi$, the initial stimulation that disappeared in the previous regime reappears gradually, albeit with weaker intensity, as shown in Fig. 4(b). Increasing the phase to $\theta = 0.5\pi$ leads to a more obvious and swift revival of the skin mode localized on the boundary, and the terminated intensity even reaches the same extent as the initial one, as shown in Fig. 4(c). This phenomenon indicates that the skin mode in the nonlinear nonreciprocal AAH model is extremely sensitive to the on-site potential, and the disappearance, emergence, and recovery of these modes can be implemented by adjusting the phase of on-site modulation.

## IV. SKIN MODES AND INTENSITY AMPLIFICATION IN THE LONG-RUN REGIME

### A. The incomplete end breather in prolonged evolution

Now we focus on the behavior of skin modes in the long-run regime. Notably, previous research [32,38,42] neglected a significant problem, in which the dynamic behavior of stimulation in the long-run regime may be different from that in the short-run case. Therefore, we explore the behavior of the end breather-like with a longer evolution, as shown in Fig. 5(a). One interesting thing is that although the end breather-like is in perfect agreement with the result in Fig. 3(c) at the beginning, the periodic oscillating end mode no longer holds its previous form, and a clear divide appears when the evolution time is prolonged. Furthermore, for clarity, we also demonstrate the intensity of the stimulated site on the boundary, as shown in Fig. 5(b). The seemingly obvious fact that the periodic oscillating end mode exists in only the first lattice site in the short-run regime and the end breather becomes unstable and decays when the evolution is prolonged to $t \approx 250$ can be confirmed, corroborating the result in Fig. 5(a). We also demonstrate the behavior of the end breather proposed in Ref. [38] in Fig. 7(a) in Appendix A and find that the end breather begins to decay and becomes chaotic in the long-run regime. The same conclusion that the theory of the end breather is not precise in the long-run regime and is applicable only on a short timescale can be drawn from the behavior of these end modes in the long-run regime. When introducing relative errors with a linear or nonlinear scaling mechanism, the system dynamics also exhibit numerous intriguing phenomena (see the details in Appendix B). Significantly, the critical time for the transition from the end breather-like region to the "vanishing breather" region remains consistent in the vicinity of $t = 250$ when the time step of the simulation is appropriately amplified (minified); the details are given in Appendix C. From our perspective, the breakdown of the end breather theory is closely related to the symmetry and non-Hermiticity of the system. The introduction of nonlinearity does not initially destroy the symmetry of the system, and the system itself still maintains a relatively complete symmetry. However, with increasing evolution time, the influence of nonlinearity gradually extends to the rest of the lattice sites and eventually leads to the breaking of the symmetry and the disappearance of the periodic oscillating end modes.

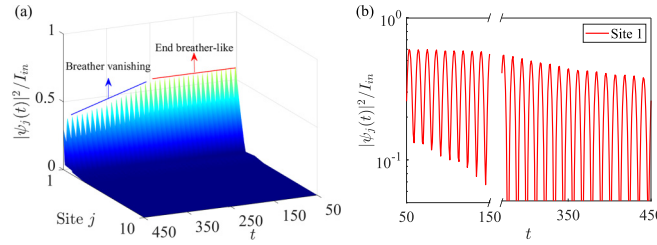


FIG. 5. The evolution of intensity with edge-site stimulation for the nonlinear AAH model. (a) The distribution of intensity under the red line represents the topological end breather-like in the short-run regime, and the distribution of intensity under the blue line denotes the vanishing of the breather when $t \geqslant 250$. (b) The evolution of intensity of the stimulated site in the long-run evolution regime. The omitted time interval is $t \in [150, 270]$. (a) and (b) have the same parameter conditions as Fig. 3(c), but for longer evolution time.

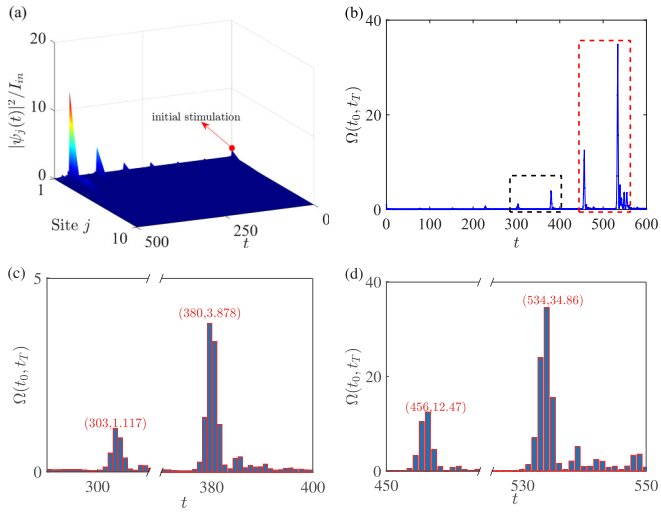


FIG. 6. (a) The evolution of intensity with edge-site stimulation in the long-run regime. (b) The relationship between the intensification factor and evolution time for the nonlinear AAH model with edge-site stimulation. (c) and (d) show the sections surrounded by black and red dotted lines in (b), respectively. The set $(x, y)$ denotes a data point of the evolution time and intensification factor. The omitted time intervals are $t \in [310, 370]$ in (c) and $t \in [465, 525]$ in (d). Here, the parameters are set as $v = 0.5$, $\Delta = 0.4$, $\alpha = 0.4$, $\kappa_0 = 0$, $\kappa_s = 0.5$, $\theta = 0.5\pi$, and $j = 1$ in [(a)–(d)].

### B. Topological intensity amplifier induced by nonlinear hopping

Next, we explore the other type of skin modes in the long-run regime. In Fig. 6(a), we demonstrate the behavior of a pattern of skin modes similar to that in Fig. 3(a), but with a longer evolution time. We can see that the occupied intensity of the initial stimulated site is extensively enhanced with increasing evolution time. To highlight the disparities between the initial and final occupied intensities of the edge site, we introduce an intensification factor denoted by $\Omega(t_0, t_T)$. This factor measures the ratio of the intensity at the final time $t_T = T$ to the intensity at the initial time $t_0 = 0$, which is defined as

$$\Omega(t_0, t_T) = \frac{|\psi_j(t_T)|^2/I_{\text{in}}}{|\psi_j(t_0)|^2/I_{\text{in}}}, \tag{4}$$

where $|\psi_j(t_T)|^2$ and $|\psi_j(t_0)|^2$ correspond to the intensities at the final and initial evolution times for site $j$, respectively. The relationship between the intensification factor and evolution time is depicted in Fig. 6(b), where no intensity amplification effect exists in $0 < t < 300$ in the short-run regime. With increasing evolution time, a result slightly greater than the initial intensity occurs at $t = 303$, and the intensification factor $\Omega(t_0, t_T)$ reaches 3.87 at $t = 380$, as shown in Fig. 6(c). Despite the amplification effect, we can see that it is not obvious when the evolution time is not long enough. Notably, the intensity amplification effect becomes obvious, and the intensification factor $\Omega(t_0, t_T)$ reaches 12.47 and 34.86 at $t = 456$ and $t = 534$, respectively, as shown in Fig. 6(d). Our results demonstrate that the introduction of nonlinearity induces the intensity amplification of the initial stimulation in the long-run regime, which originates from the combination effect of the nonlinear hopping and NHSEs. Particularly, this result also illustrates that the nonlinearity can generate new types of boundary states while supporting the amplification effect of edge-site stimulation. Moreover, this phenomenon holds universally; this amplification effect can also be found in Ref. [38] in the long-run regime, and the amplification effect is also demonstrated in Fig. 7(b) in Appendix A. These findings could be useful in designing topological devices for quantum information processing, such as topological amplifiers and topological repeaters.

## V. CONCLUSIONS

In conclusion, we studied the extended nonreciprocal non-Hermitian AAH lattice and explored the topological soliton states and intensity amplification induced by nonlinearity. The phase boundaries between the Anderson localized and skin phases were demonstrated, which serves as a foundation for exploring the impact of nonlinearity on the topological characteristics under non-Hermitian conditions. The analysis of the site intensity evolution under open boundary conditions revealed that nonlinearity can induce multiple types of skin modes. We examined how the on-site potential affects the behavior of skin modes to explore the characteristics of these skin modes in nonlinear systems. Our findings revealed that changing the phase of on-site modulation can lead to the vanishing, appearance, and recovery of a skin mode localized at the boundary. Moreover, it was found that the end breather-like no longer maintains a stable oscillating form in the long-run regime. The edge-site intensity at the end of evolution was significantly stronger than that at the beginning of evolution; this counterintuitive phenomenon was also observed in previous work, such as Ref. [38]. Furthermore, a time-dependent intensification factor was investigated, and it was found that the amplification effect is more pronounced in the long-run regime. Our work provides insight into novel skin modes induced by nonlinearity in a non-Hermitian lattice and the intensity amplification in the prolonged evolution regime, highlighting the important potential of nonlinear topological systems for topological intensity amplifiers and repeaters.

## ACKNOWLEDGMENT

This work was supported by the National Natural Science Foundation of China under Grants No. 12074330, No. 62071412, and No. 12074094.

## APPENDIX A: THE INCOMPLETE TOPOLOGICAL END BREATHER IN THE LONG-RUN REGIME

In this Appendix, we demonstrate the time evolution of site intensities for the SSH-type lattice with both nonlinearity and nonreciprocal non-Hermiticity proposed in Ref. [38]. The non-Hermitian Hamiltonian for this lattice is expressed as follows:

$$H_{\text{SSH}} = \sum_{n=1,2,\ldots} [(\kappa + \gamma_n)a_{2n-1}^\dagger a_{2n} + (\kappa - \gamma_n)a_{2n}^\dagger a_{2n-1} + v(a_{2n}^\dagger a_{2n+1} + a_{2n+1}^\dagger a_{2n})], \tag{A1}$$

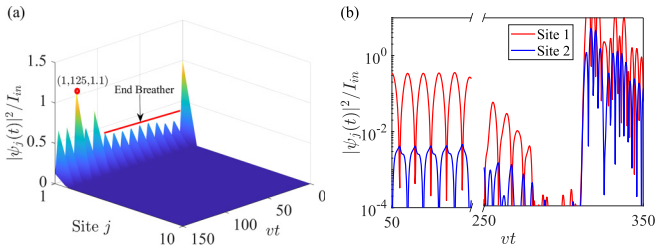


FIG. 7. The evolution of intensity with edge-site stimulation for the nonlinearity SSH model with the same parameter conditions as in Ref. [38] but longer evolution time. (a) The distribution of intensity under the red line represents the topological end breather in the short-run regime, and the breather breaks when $vt \geqslant 103$. (b) The evolution of the intensity of the edge cell in the long-run evolution regime. The red (blue) line denotes the intensity in the first site (second site) in the first cell. The omitted time interval is $vt \in [100, 250]$. Other parameters are set as $\gamma_0 = 0$, $\gamma_s = \sqrt{7}/2$, $\kappa = \sqrt{2}$, and $v = 1$ in both (a) and (b).

where $a_j^{(\dagger)}$ denotes the annihilation (creation) operator on site $j$, $\kappa \pm \gamma_n$ denotes intracell nonreciprocal hopping, and $v$ are the reciprocal intercell hoppings. They have the same forms of the initial state and stimulation as in Ref. [38]. This work identifies specific topological end breathers that appear in certain parameter regimes. The intrinsic cause of these end breathers is derived from the competition between intracell nonlinearity and intercell reciprocity hopping, which induces an alternating appearance of localized boundary states and generates the end breather on a short timescale.

However, this conclusion seems applicable only on a short-term scale. To demonstrate this phenomenon, we present the topological end breather in Fig. 7(a), but with a longer evolution time. The short-run end breather is in perfect agreement with the result in Ref. [38]. Notably, the periodic and harmonious end breather breaks down when the evolution time is prolonged. Moreover, we also demonstrate the intensity of two lattice sites on the edge, as shown in Fig. 7(b). The fact that the end breather exists at the first lattice site in the short-run regime can be confirmed, but the end breather becomes unstable and chaotic when evolution is prolonged to $vt \approx 250$, which indicates that the theory of end breathers is not precise in the long-run regime. Furthermore, the intensity at the first site is enhanced in the prolonged evolution regime, where the intensity of the first site is far beyond the initial one, as shown in the right half of Fig. 7(b). The above findings indicate that the end breather no longer maintains its form in the short-run regime and the amplification effect of edge-site stimulation appears in the long-run regime.

## APPENDIX B: THE DYNAMICAL BEHAVIORS WITH LINEAR AND NONLINEAR NUMERICAL ERRORS

Here, we define the relative errors of each evolution unit step $t_{\text{step}}$ as fluctuating values, represented as $t_{\text{step}} \pm \delta$ ($\delta = \text{random}[0, x], x \in (0, 1)$). By adjusting this parameter, we can effectively regulate the extent of the relative error and its impact on the end breather's behavior. The relative error is influenced by the number of evolutionary steps, denoted as $f(n)$, where $n$ represents the evolution steps. We can define the unit evolution time as $\widetilde{t_n} = t_{\text{step}} \pm \delta f(n)$. The relative error can take various forms, including a linear scaling form when $f(n) = kn + C$ ($k$ and $C$ are both constants) and nonlinear scaling forms in terms of $f(n) = \sqrt{n}$ and $f(n) = n^2$, as well as other distinct patterns.

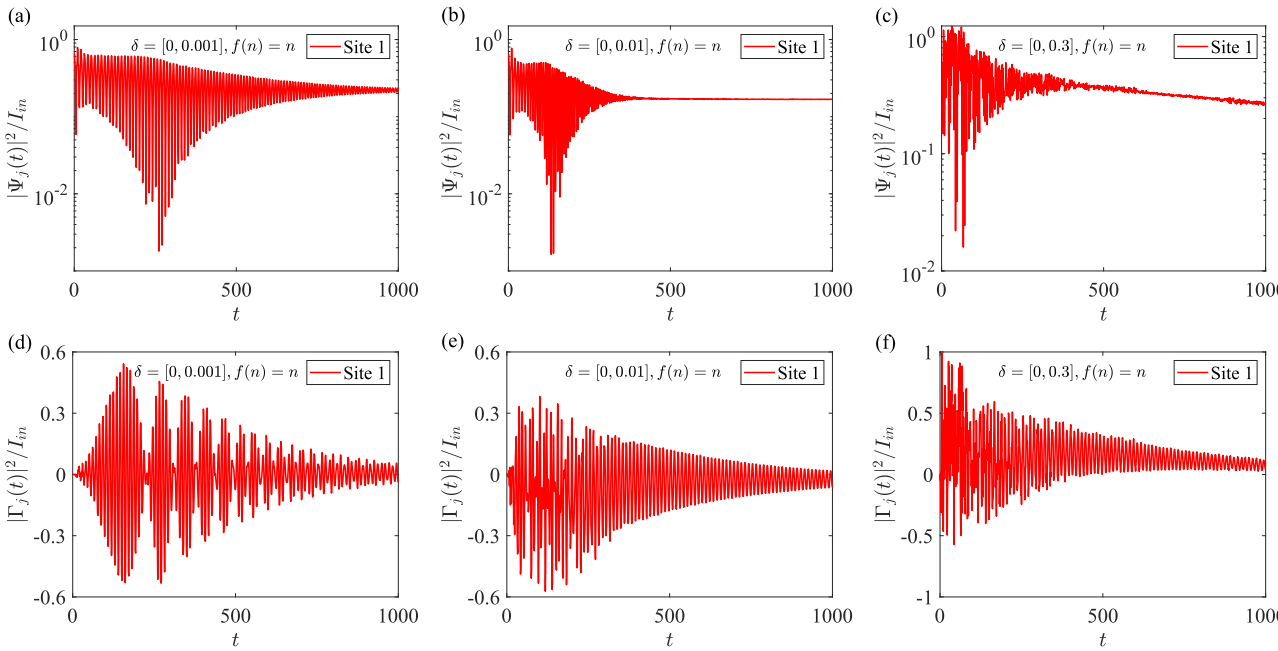


FIG. 8. The evolution of intensity $|\Psi_j(t)|^2/I_{\text{in}}$ and the relative numerical errors $|\Gamma_j(t)|^2/I_{\text{in}}$ under different linear error scaling forms $f(n) = n$. [(a)–(c)] correspond to different amplitudes of fluctuations, with $\delta = [0, 0.001]$, $\delta = [0, 0.01]$, and $\delta = [0, 0.3]$, respectively. [(d)–(f)] show the magnitude of the numerical errors. The parameters are determined as $\kappa_0 = 0.3$, $\kappa_s = 0.7$, $\Delta = 3.2$, $\alpha = 3/10(\sqrt{5} - \sqrt{3})$, $v = 1$, and $\theta = 1.41\pi$.

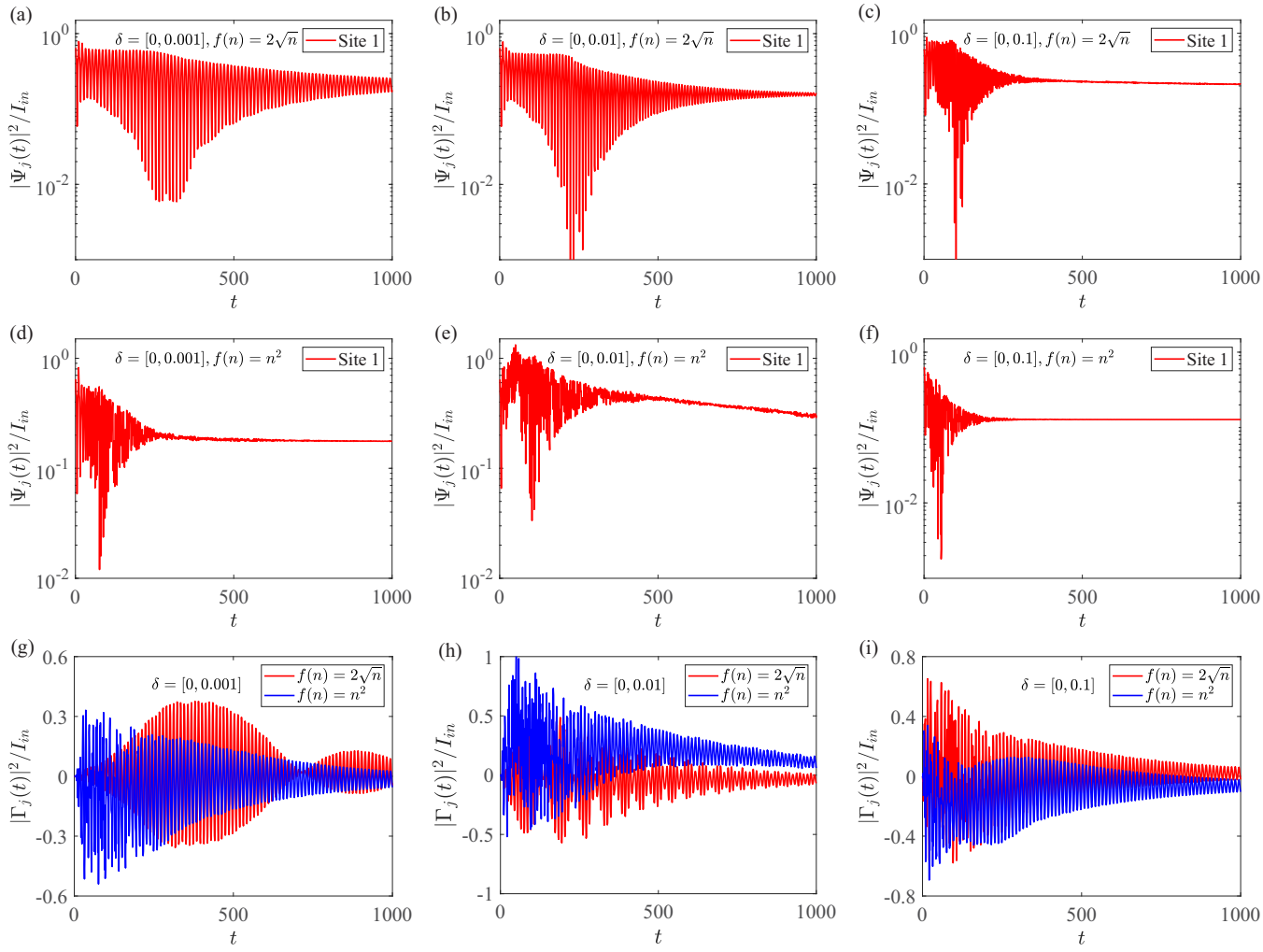


FIG. 9. The evolution of intensity $|\Psi_j(t)|^2/I_{\text{in}}$ and the relative numerical errors $|\Gamma_j(t)|^2/I_{\text{in}}$ under different nonlinear error scaling forms: [(a)–(c)] $f(n) = 2\sqrt{n}$ and [(d)–(f)] $f(n) = n^2$. [(a)–(c)] and [(d)–(f)] correspond to different amplitudes of fluctuations, with $\delta = [0, 0.001]$, $\delta = [0, 0.01]$, and $\delta = [0, 0.1]$, respectively. [(g)–(i)] show the magnitudes of the numerical errors. The red and blue lines correspond to the nonlinearly scaling forms $f(n) = 2\sqrt{n}$ and $f(n) = n^2$, respectively. The parameters are the same as in Fig. 8.

For the linearly scaling mechanism, we delve into the influence of relative errors on the dynamical behaviors exhibited by the system. The evolution of intensities governed by the linearly scaling function $f(n) = n$ is visually represented in Figs. 8(a)–8(c), accompanied by distinct amplitudes of fluctuations $\delta$. Notably, for relatively small amplitudes of fluctuations $\delta = [0, 0.001]$, as depicted in Fig. 8(a), the intensity distribution continues to exhibit oscillatory forms akin to the case without fluctuations. However, when the amplitude of fluctuations increases to $\delta = [0, 0.01]$ and $\delta = [0, 0.3]$, as demonstrated in Figs. 8(b) and 8(c), the intensity distribution deviates from stable oscillations and enters a regime of chaotic dynamics. This phenomenon highlights that the introduction of linear fluctuations disrupts the oscillatory behavior of the end breather-like. Furthermore, we investigate the behaviors of numerical errors under multiple iteration steps in Figs. 8(d)–8(f). Here, $|\Psi_j(t)|^2/I_{\text{in}}$ and $|\psi_j(t)|^2/I_{\text{in}}$ represent the intensity evolution with and without relative errors, respectively. The numerical errors associated with the simulated time step are denoted as $|\Gamma_j(t)|^2/I_{\text{in}} = |\Psi_j(t)|^2/I_{\text{in}} - |\psi_j(t)|^2/I_{\text{in}}$. When the amplitude of fluctuation is small, the error manifests in a manner resembling Rabi oscillations, as depicted in Fig. 8(d). However, as the amplitude of fluctuation increases, the relative error of the system becomes more intricate during the initial stages of evolution but gradually converges over an extended evolution time, as illustrated in Figs. 8(e) and 8(f).

Now, we pay attention to the relative errors characterized by a weak nonlinear scaling mechanism, denoted as $f(n) = 2\sqrt{n}$ and depicted in Figs. 9(a)–9(c), and a strong nonlinear scaling form, denoted as $f(n) = n^2$ and shown in Figs. 9(d)–9(f), considering various fluctuation amplitudes $\delta$. Notably, when $\delta$ takes values within the ranges of $\delta = [0, 0.001]$ and $\delta = [0, 0.01]$, as depicted in Figs. 9(a) and 9(b), the intensity evolution of the system consistently retains an oscillatory form. Only when the amplitude of fluctuation surpasses a certain threshold, for instance, $\delta = [0, 0.1]$, as shown in Fig. 9(c), does the intensity distribution of the system transition into a chaotic regime. Our observations reveal that the relative errors limit sensitivity to weak nonlinear scaling.

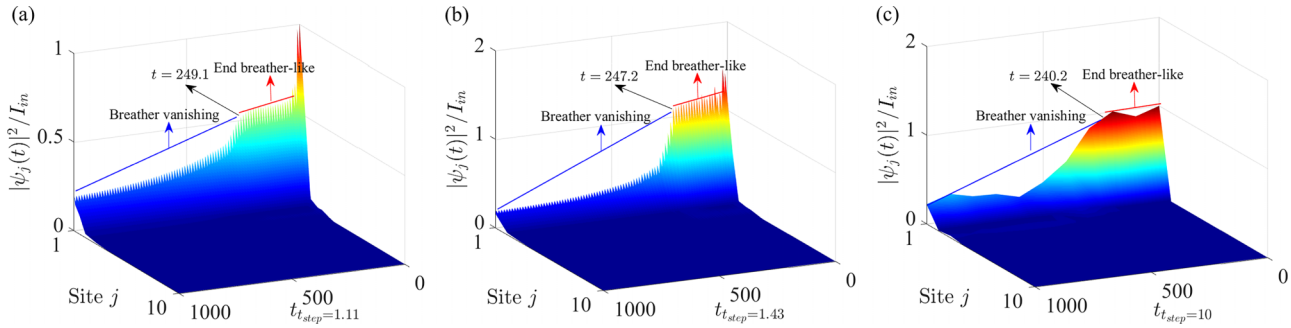


FIG. 10. The evolution of the intensity with edge-site stimulation for different amplified time steps of the simulation. [(a)–(c)] show the dynamical behaviors with time steps of the simulation $t_{\text{step}} = 1000/900 = 1.11$, $t_{\text{step}} = 1000/700 = 1.43$, and $t_{\text{step}} = 1000/100 = 10$, respectively. Here, the parameters are determined to be $\kappa_0 = 0.3$, $\kappa_s = 0.7$, $\Delta = 3.2$, $\alpha = 3/10(\sqrt{5} - \sqrt{3})$, $\nu = 1$, and $\theta = 1.41\pi$ in [(a)–(c)].

The situation takes a distinct turn when we consider the strong nonlinear scaling mechanism, which is evident in Figs. 9(d)–9(f). Furthermore, we quantify the numerical error associated with the simulated time step in Figs. 9(g)–9(i), with the red and blue lines representing the nonlinear scaling forms $f(n) = 2\sqrt{n}$ and $f(n) = n^2$, respectively. In line with the observations made for the linearly scaling case, we find that the relative errors gradually converge over prolonged evolution times, irrespective of their distinct error evolution forms.

## APPENDIX C: THE DYNAMICAL BEHAVIORS WITH MAGNIFIED OR MINIFIED EVOLUTIONARY STEPS

It is crucial to provide clarification of the definition of the unit time step in the simulation in the main text. We define the unit time step as $t_{\text{step}} = \frac{T}{N_T}$, where $T$ represents the total evolution time and $N_T$ denotes the number of intervals. In our study, we specifically set $T = N_T$, resulting in a unit time step of $t_{\text{step}} = 1$ within our analysis. It is noteworthy that a distinct divergence in behavior is observed between the end breather-like and vanishing breather phenomena, particularly around $t = 250$. Based on the preceding information, we delve into the behavior of the critical time $t_c$ when the time step of the simulation is either minified or magnified. Notably, the relationship between the total evolutionary time $T_{\text{total}}$ and evolutionary step $t_{\text{step}}$ along with the number of steps $N_{\text{total}}$ can be expressed as $T_{\text{total}} = t_{\text{step}} N_{\text{total}}$, which signifies that the representation of evolutionary time is no longer solely reliant on the discrete count of evolutionary steps, but rather takes the form of $t_{\text{step}} N_T$, particularly when $t_{\text{step}} \neq 1$.

For the magnified case, we explore the scenario where the unit evolutionary step is magnified, with fixed total evolution time $T = 1000$ but varying interval numbers. Drawing from the aforementioned analysis, we demonstrate the dynamical behavior of the system in the case of a magnified evolutionary step. Specifically, we focus on the cases where $t_{\text{step}} = 1000/900 = 1.11$, $t_{\text{step}} = 1000/700 = 1.43$, and $t_{\text{step}} = 1000/100 = 10$ in Figs. 10(a)–10(c), respectively. Our results reveal that the critical time for the transition from end breather-like to vanishing breather is around $t_c = 250$, which indicates the magnification of the step does not significantly affect the critical evolution time $t_c$. Regarding the scenario with the minified step, we delve into cases where $t_{\text{step}} = 1000/1100 = 0.91$, $t_{\text{step}} = 1000/1800 = 0.55$, and $t_{\text{step}} = 1000/10000 = 0.1$ in Figs. 11(a)–11(c), respectively. Within the scope of these findings, we have observed analogous outcomes, where the critical evolution time remains in the vicinity of $t = 250$, despite minor deviations. Although there are slight discrepancies in their critical times, they remain on the same order of magnitude, implying that this phenomenon arises from the evolution of a nonlinear system. This suggests that such variations are unlikely to exert a substantial impact on the physical behavior of the system. Consequently, we conclude that appropriate magnification or minification of the evolutionary steps will not have a significant impact on the critical time $t_c$.

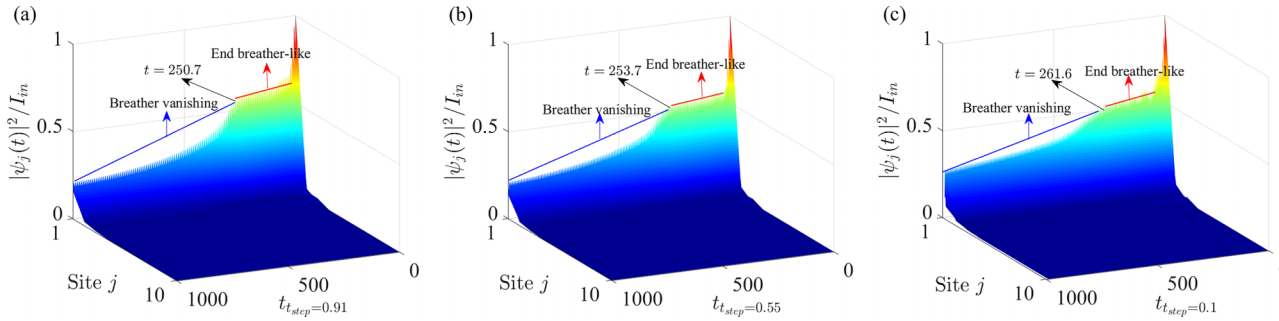


FIG. 11. The evolution of the intensity with edge-site stimulation for different minified time steps of the simulation. (a)–(c) show the dynamical behaviors with time steps of the simulation $t_{\text{step}} = 1000/1100 = 0.91$, $t_{\text{step}} = 1000/1800 = 0.55$, and $t_{\text{step}} = 1000/10000 = 0.1$, respectively. The parameters are the same as in Fig. 10.

[1] C. L. Kane and E. J. Mele, $Z_2$ Topological Order and the Quantum Spin Hall Effect, Phys. Rev. Lett. **95**, 146802 (2005).

[2] B. A. Bernevig, T. L. Hughes, and S. C. Zhang, Quantum spin Hall effect and topological phase transition in HgTe quantum wells, Science **314**, 1757 (2006).

[3] L. Fu, C. L. Kane, and E. J. Mele, Topological Insulators in Three Dimensions, Phys. Rev. Lett. **98**, 106803 (2007).

[4] M. Z. Hasan and C. L. Kane, Colloquium: Topological insulators, Rev. Mod. Phys. **82**, 3045 (2010).

[5] X. L. Qi and S. C. Zhang, Topological insulators and superconductors, Rev. Mod. Phys. **83**, 1057 (2011).

[6] M. A. Metlitski, C. L. Kane, and M. P. A. Fisher, Bosonic topological insulator in three dimensions and the statistical Witten effect, Phys. Rev. B **88**, 035131 (2013).

[7] H. Shen, B. Zhen, and L. Fu, Topological Band Theory for Non-Hermitian Hamiltonians, Phys. Rev. Lett. **120**, 146402 (2018).

[8] S. Yao, F. Song, and Z. Wang, Non-Hermitian Chern Bands, Phys. Rev. Lett. **121**, 136802 (2018).

[9] Z. P. Gong, Y. Ashida, K. Kawabata, K. Takasan, S. Higashikawa, and M. Ueda, Topological Phases of Non-Hermitian Systems, Phys. Rev. X **8**, 031079 (2018).

[10] X. X. Bao, G. F. Guo, and L. Tan, Exploration of the topological properties in a non-Hermitian long-range system, J. Phys.: Condens. Matter **33**, 465403 (2021).

[11] N. Okuma, K. Kawabata, K. Shiozaki, and M. Sato, Topological Origin of Non-Hermitian Skin Effects, Phys. Rev. Lett. **124**, 086801 (2020).

[12] L. Jin and Z. Song, Bulk-boundary correspondence in a non-Hermitian system in one dimension with chiral inversion symmetry, Phys. Rev. B **99**, 081103(R) (2019).

[13] H. Jiang, L. J. Lang, C. Yang, S. L. Zhu, and S. Chen, Interplay of non-Hermitian skin effects and Anderson localization in nonreciprocal quasiperiodic lattices, Phys. Rev. B **100**, 054301 (2019).

[14] Z. X. Zhang, R. Huang, L. Qi, Y. Xing, Z. J. Zhang, and H. F. Wang, Topological phase transition and eigenstates localization in a generalized non-Hermitian Su-Schrieffer-Heeger model, Ann. Phys. **533**, 2000272 (2020).

[15] J. Cao, X. X. Yi, and H. F. Wang, Band structure and the exceptional ring in a two-dimensional superconducting circuit lattice, Phys. Rev. A **102**, 032619 (2020).

[16] S. Longhi, Phase transitions in a non-Hermitian Aubry-André-Harper model, Phys. Rev. B **103**, 054203 (2021).

[17] S. Longhi, Self-Healing of Non-Hermitian Topological Skin Modes, Phys. Rev. Lett. **128**, 157601 (2022).

[18] Y. Ashida, Z. Gong, and M. Ueda, Non-Hermitian physics, Adv. Phys. **69**, 249 (2020).

[19] S. Yao and Z. Wang, Edge States and Topological Invariants of Non-Hermitian Systems, Phys. Rev. Lett. **121**, 086803 (2018).

[20] C. H. Lee and R. Thomale, Anatomy of skin modes and topology in non-Hermitian systems, Phys. Rev. B **99**, 201103(R) (2019).

[21] F. K. Kunst, E. Edvardsson, J. C. Budich, and E. J. Bergholtz, Biorthogonal Bulk-Boundary Correspondence in Non-Hermitian Systems, Phys. Rev. Lett. **121**, 026808 (2018).

[22] V. M. Martinez Alvarez, J. E. Barrios Vargas, and L. E. F. Foa Torres, Non-Hermitian robust edge states in one dimension: Anomalous localization and eigenspace condensation at exceptional points, Phys. Rev. B **97**, 121401(R) (2018).

[23] D. Leykam, K. Y. Bliokh, C. Huang, Y. D. Chong, and F. Nori, Edge Modes, Degeneracies, and Topological Numbers in Non-Hermitian Systems, Phys. Rev. Lett. **118**, 040401 (2017).

[24] L. Qi, G. L. Wang, S. Liu, and H. F. Wang, Robust interface-state laser in non-Hermitian micro-resonator arrays, Phys. Rev. Appl. **13**, 064015 (2020).

[25] Y. Xing, L. Qi, X. D. Zhao, Z. Lu, S. Liu, S. Zhang, and H. F. Wang, Quantum transport in a one-dimensional quasicrystal with mobility edges, Phys. Rev. A **105**, 032443 (2022).

[26] S. Xia, D. Kaltsas, D. Song, I. Komis, J. Xu, A. Szameit, H. Buljan, K. G. Makris, and Z. Chen, Nonlinear tuning of PT symmetry and non-Hermitian topological states, Science **372**, 72 (2021).

[27] L. W. Zhou and J. B. Gong, Non-Hermitian Floquet topological phases with arbitrarily many real-quasienergy edge states, Phys. Rev. B **98**, 205417 (2018).

[28] M. S. Rudner and N. H. Lindner, Band structure engineering and non-equilibrium dynamics in Floquet topological insulators, Nat. Rev. Phys. **2**, 229 (2020).

[29] C. Yin, H. Jiang, L. Li, R. Lü, and S. Chen, Geometrical meaning of winding number and its characterization of topological phases in one-dimensional chiral non-Hermitian systems, Phys. Rev. A **97**, 052115 (2018).

[30] C. W. Lee, P. Kurzyński, and N. Hyunchul, Quantum walk as a simulator of nonlinear dynamics: Nonlinear Dirac equation and solitons, Phys. Rev. A **92**, 052336 (2015).

[31] L. J. Lang, Y. J. Wend, Y. H. Zhang, E. H. Cheng, and Q. X. Liang, Dynamical robustness of topological end states in nonreciprocal Su-Schrieffer-Heeger models with open boundary conditions, Phys. Rev. B **103**, 014302 (2021).

[32] Y. Hadad, A. B. Khanikaev, and A. Alù, Self-induced topological transitions and edge states supported by nonlinear staggered potentials, Phys. Rev. B **93**, 155112 (2016).

[33] A. Prasad, M. Dhamala, B. M. Adhikari, and R. Ramaswamy, Amplitude death in nonlinear oscillators with nonlinear coupling, Phys. Rev. E **81**, 027201 (2010).

[34] W. P. Su, J. R. Schrieffer, and A. J. Heeger, Solitons in Polyacetylene, Phys. Rev. Lett. **42**, 1698 (1979).

[35] Y. V. Kartashov, B. A. Malomed, and L. Torner, Solitons in nonlinear lattices, Rev. Mod. Phys. **83**, 247 (2011).

[36] B. F. Zhu, Q. Wang, D. Leykam, H. Xue, Q. J. Wang, and Y. D. Chong, Anomalous Single-Mode Lasing Induced by Nonlinearity and the Non-Hermitian Skin Effect, Phys. Rev. Lett. **129**, 013903 (2022).

[37] P. M. Gunnink, B. Flebus, H. M. Hurst, and R. A. Duine, Nonlinear dynamics of the non-Hermitian Su-Schrieffer-Heeger model, Phys. Rev. B **105**, 104433 (2022).

[38] L. J. Lang, S. L. Zhu, and Y. D. Chong, Non-Hermitian topological end breathers, Phys. Rev. B **104**, L020303(R) (2021).

[39] K. Mochizuki, K. Mizuta, and N. Kawakami, Fate of topological edge states in disordered periodically driven nonlinear systems, Phys. Rev. Res. **3**, 043112 (2021).

[40] T. L. Heugel, O. Zilberberg, C. Marty, R. Chitra, and A. Eichler, Ising machines with strong bilinear coupling, Phys. Rev. Res. **4**, 013149 (2022).

[41] H. Zhao, P. Miao, M. Teimourpour, S. Malzard, R. El-Ganainy, H. Schomerus, and L. Feng, Topological hybrid silicon microlasers, Nat. Commun. **9**, 981 (2018).

[42] M. Ezawa, Nonlinear non-Hermitian higher-order topological laser, Phys. Rev. Res. **4**, 013195 (2022).

[43] S. Kruk, A. Poddubny, D. Smirnova, L. Wang, A. Slobozhanyuk, A. Shorokhov, I. Kravchenko, B. Luther-Davies, and Y. Kivshar, Nonlinear light generation in topological nanostructures, Nat. Nanotechnol. **14**, 126 (2019).

[44] M. J. Ablowitz, C. W. Curtis, and Y. P. Ma, Linear and nonlinear traveling edge waves in optical honeycomb lattices, Phys. Rev. A **90**, 023813 (2014).

[45] Y. F. Wang, J. H. Zhang, Y. Q. Li, J. Z. Wu, W. L. Liu, F. Mei, Y. Hu, L. T. Xiao, J. Ma, C. Chin, and S. T. Jia, Observation of Interaction-Induced Mobility Edge in an Atomic Aubry-André Wire, Phys. Rev. Lett. **129**, 103401 (2022).

[46] Y. Wang, L. J. Lang, C. H. Lee, B. L. Zhang, and Y. D. Chong, Topologically enhanced harmonic generation in a nonlinear transmission line metamaterial, Nat. Commun. **10**, 1102 (2019).

[47] Y. Lumer, Y. Plotnik, M. C. Rechtsman, and M. Segev, Self-Localized States in Photonic Topological Insulators, Phys. Rev. Lett. **111**, 243905 (2013).

[48] D. Leykam and Y. D. Chong, Edge Solitons in Nonlinear-Photonic Topological Insulators, Phys. Rev. Lett. **117**, 143901 (2016).

[49] H. Xue, Y. Yang, F. Gao, Y. Chong, and B. Zhang, Acoustic higher-order topological insulator on a kagome lattice, Nat. Mater. **18**, 108 (2019).

[50] J. Li, A. K. Harter, J. Liu, L. de Melo, Y. N. Joglekar, and L. Luo, Observation of parity-time symmetry breaking transitions in a dissipative Floquet system of ultracold atoms, Nat. Commun. **10**, 855 (2019).

[51] S. Aubry and G. André, Analyticity breaking and Anderson localization in incommensurate lattices, Ann. Israel Phys. Soc. **3**, 18 (1980).

[52] K. K. Das and J. Christ, Realizing the Harper model with ultracold atoms in a ring lattice, Phys. Rev. A **99**, 013604 (2019).